PHYSICAL REVIEW B VOLUME 35, NUMBER 12 15 APRIL 1987-II

Moving discommensurations interacting with diffusing impurities

D. J. Srolovitz and R. Eykholt
Los Alamos National Laboratory, Los Alamos, New Mexico 87545

D. M. Barnett
Department of Materials Science and Engineering, Stanford University, Stanford, California 94305

J. P. Hirth
Department of Metallurgical Engineering, Ohio State University, Columbus, Ohio 43210
(Received 3 November 1986)

We present an analytical description of the interaction between moving discommensurations and diffusing impurities for a realistic form of the impurity-discommensuration interaction energy. This interaction energy is derived within the framework of the modified sine-Gordon model with either misfit impurities (coupling to the gradient of the order parameter) or elastic-modulus impurities (coupling directly to the order parameter). This interaction potential is then employed in calculating the steady-state impurity concentration profile about the moving discommensuration for arbitrary discommensuration velocity and impurity diffusivity. The impurities provide a drag force on the moving discommensuration, which may lead to hysteresis in the relation between the applied force and the discommensuration velocity. Analytic results for the onset of hysteresis, as well as for the velocities and forces delimiting the hysteretic regime, are presented. Finally, we apply these results to charge-density waves, ferroelectric domain walls, and grain boundaries.

I. INTRODUCTION

The interactions of impurities with discommensurations or discommensuration-like defects often controls the microstructure and/or transport properties of a material. The role of impurities in the dynamics of charge-density waves,[1,2] domain walls in ferroelectrics,[3] and grain boundaries in polycrystalline materials[4] has received considerable attention both experimentally[1-4] and theoretically.[5-9] The majority of these theoretical analyses have concentrated on the interactions of discommensurations with static impurities. Of particular note is a study by Fogel *et al.*[5] in which they considered the effect of static impurities which couple to the gradient of the order parameter on the dynamics of solitons in the one-dimensional sine-Gordon model. They found that, at low velocities, the soliton was trapped by the impurities, while, at high velocities, the soliton was essentially unaffected (apart from a phase shift). Observations of grain boundaries in metals[4] show similar impurity pinning at low velocities, and little or no effect at high velocities.

When the impurities are free to diffuse, the meaning of pinning becomes ambiguous. At low discommensuration velocity, the impurities are capable of diffusing along with the moving discommensurations. This results in a nonrandom spatial distribution of impurities, and a retarding, "frictional" force on the discommensurations. On the other hand, at large discommensuration velocity, the impurities cannot diffuse at a sufficient rate to keep up with the discommensurations, and, hence, the impurity distribution is only slightly perturbed, and the retarding force is negligible. Clearly, the retarding force is a complicated function of the discommensuration velocity, and, thus, these systems may exhibit hysteresis as the applied field is varied. These observations are consistent with the qualitative description given by Cahn[9] of the effect of impurities on moving grain boundaries.

The purpose of the present paper is to provide an analytical description of the interaction between moving discommensurations and diffusing impurities for a realistic form of the impurity-discommensuration interaction energy. In Sec. II of this paper, we obtain a simple expression for the interaction potential between discommensurations and impurities in a modified sine-Gordon model. Two types of impurities are considered: one coupling directly to the order parameter, and the other coupling to its gradient. These expressions for the interaction potential are then employed in Sec. III to obtain the steady-state impurity concentration about a moving discommensuration. The drag force on the discommensuration caused by these impurities is then calculated in Sec. IV, and employed in Sec. V to obtain an analytic relationship between the applied force and the discommensuration velocity. Finally, we calculate the magnitude of the hysteresis in this force-velocity relationship, and we find the conditions for its onset. Applications of these results to the dynamics of charge-density waves, ferroelectric domain walls, and grain boundaries are also discussed.

II. IMPURITY-DISCOMMENSURATION INTERACTION POTENTIALS

The physical nature of the interaction between impurities and discommensurations may be elucidated best in terms of a simple model. Because of its widespread application to a number of physical systems and its simple con-

tinuum limit, we begin with the Frenkel-Kontorova model:[10]

$$H=\tfrac{1}{2}\Sigma_i\{m(\partial r_i/\partial t)^2+K_i(r_{i+1}-r_i-\alpha_i)^2 +2B_i[1-\cos(2\pi r_i/a_0)]\}\ , \tag{2.1}$$

where r_i is the displacement field of the particles of mass m, a_0 is the lattice spacing, K_i is the spring constant, B_i is the amplitude of the substrate potential, and α_i is a phase-shift parameter. Three types of impurities are considered: (a) a spring whose equilibrium length is incommensurate with the substrate potential (some $\alpha_i\neq 0$), (b) a local variation in spring constant (some $K_i\neq K$), and (c) a local variation in the amplitude of the substrate potential (some $B_i\neq B$). The natures of these types of impurities are indicated in Fig. 1. Case (a) corresponds to a misfit impurity. Cases (b) and (c) may be interpreted as impurities with elastic constants differing from those of the rest of the medium. In the static limit, rescaling the Hamiltonian by K reduces the two cases (b) and (c) to just one type of elastic-constant defect controlled by the parameter $(B/K)_i$. In the static, continuum limit, Eq. (2.1) becomes

$$H=\tfrac{1}{2}\int_{-\infty}^{\infty}\{[\phi_u(u)-\Delta(u)]^2+2\beta(u)[1-\cos\phi(u)]\}du\ , \tag{2.2}$$

where $u=x/a_0$ is the dimensionless position, $\phi(u)$ is the continuum displacement (phase) variable, $\phi_u(u)=\partial\phi(u)/\partial u$, $\beta=4\pi^2B/Ka_0^2$, and $\Delta=2\pi\alpha/a_0$. Note that the Hamiltonian in Eq. (2.2) has been rescaled by $Ka_0^2/4\pi^2$.

In order to simplify the following evaluations of the impurity-discommensuration interaction potentials, we linearize (2.2), resulting in

$$H=\tfrac{1}{2}\int_{-\infty}^{\infty}\{[\phi_u(u)-\Delta(u)]^2+\beta(u)[\phi(u)\ (\mathrm{mod}\,2\pi)]^2\}du\ , \tag{2.3}$$

where $(\mathrm{mod}\,2\pi)$ has been included to maintain the 2π periodicity of H. This equation is the continuum analog of the modified Frenkel-Kontorova model used by Wiener.[11]

The equation of motion for $\phi(u)$ is obtained from Eq. (2.3) by using Hamilton's equations in the usual way, and it is given by

$$\phi_{uu}(u)-\beta(u)[\phi(u)\ (\mathrm{mod}\,2\pi)]=\Delta_u(u)\ . \tag{2.4}$$

In the absence of impurities, we have $\Delta\equiv 0$ and $\beta\equiv 1$,[12]

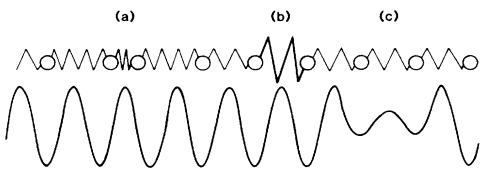

FIG. 1. Illustration of the various types of impurities considered in Sec. II. (a) Misfit impurity with atoms shifted from the minima of the substrate potential. (b) Elastic-modulus impurity with a modified interatomic interaction. (c) Elastic-modulus impurity with a modified substrate potential. Cases (b) and (c) are mathematically equivalent.

and this becomes

$$\phi_{uu}(u)-[\phi(u)\ (\mathrm{mod}\,2\pi)]=0\ , \tag{2.5}$$

which has the solution $\phi(\mathrm{u})\ (\mathrm{mod}\,2\pi)=A_1e^u+A_2e^{-u}$. To find the soliton solution, we impose the boundary conditions $\phi(-\infty)=2\pi$ and $\phi(\infty)=0$, which yields (for a soliton at $u=u_s$)

$$\phi_s(u)=\begin{cases}2\pi-\pi e^{u-u_s}, & u\leq u_s\\ \pi e^{u_s-u}, & u\geq u_s\ .\end{cases} \tag{2.6}$$

This soliton has an energy

$$H[\phi_s]=\pi^2\ , \tag{2.7}$$

which is within 20% of the soliton energy for the full sine-Gordon equation. This solution (2.6) is plotted in Fig. 2 along with the soliton solution of the full sine-Gordon equation,[10] as well as the hyperbolic-tangent form found in a Landau description of a discommensuration.[13] These three solutions show a striking similarity, and they demonstrate that the linearized sine-Gordon equation contains the essential physics required to describe discommensurations. As shown later, the expressions for the impurity-discommensuration interaction potentials obtained using the linearized sine-Gordon equation are relatively simple. The simplicity of these expressions allows us to proceed with the remainder of the analysis analytically, rather than numerically.

A. Misfit impurities

We begin by finding the displacement field ϕ_{mis} for a misfit impurity alone. The impurity profile is taken to be steplike and of extent $2u_0$, with its center at $u=0$ [i.e., $\beta\equiv 1$, $\Delta(u)=0$ for $|u|>u_0$, and $\Delta(u)=\Delta\neq 0$ for $|u|\leq u_0$]. In this case, Eq. (2.4) becomes

$$\phi_{uu}(u)-[\phi(u)\ (\mathrm{mod}\,2\pi)]=\Delta\delta(u+u_0)-\Delta\delta(u-u_0)\ , \tag{2.8}$$

which, together with the boundary conditions $\phi(\pm\infty)=0$,

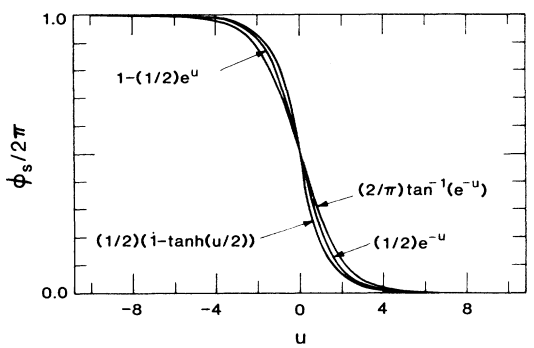

FIG. 2. Comparison of various soliton profiles. The middle curve is the soliton solution given by Eq. (2.6) with $u_s=0$. The outer curves are the soliton solution of the full sine-Gordon equation and the hyperbolic-tangent form found in a Landau description of a discommensuration.

yields

$$\phi_{\rm mis}(u)=\begin{cases} -\Delta(\sinh u_0)e^{u}, & u<-u_0 \\ \Delta e^{-u_0}\sinh u, & -u_0\le u\le u_0 \\ \Delta(\sinh u_0)e^{-u}, & u>u_0 \end{cases} \quad (2.9)$$

In addition, the energy of this impurity is

$$H[\phi_{\rm mis}]=\Delta^2 e^{-u_0}(2u_0\cosh u_0-2\sinh u_0 + e^{-u_0}\sinh^2 u_0) . \quad (2.10)$$

Next, we find the displacement field $\tilde{\phi}_{\rm mis}$ with both the soliton and the misfit impurity present. This is done by solving Eq. (2.8) with the (different) boundary conditions $\phi(-\infty)=2\pi$ and $\phi(\infty)=0$. In this particular case, we find that $\tilde{\phi}_{\rm mis}=\phi_s+\phi_{\rm mis}$. Thus, the interaction energy of a discommensuration with a misfit impurity is given by (for $|u_s|>u_0$)

$$E_{\rm mis}=H[\phi_s+\phi_{\rm mis}]-H[\phi_s]-H[\phi_{\rm mis}] =2\pi\Delta(\sinh u_0)e^{-|u_s|} , \quad (2.11)$$

with u_s being the (dimensionless) impurity-discommensuration separation (since the impurity is at $u=0$). The interaction energy scales linearly with the impurity strength Δ, and decays exponentially with the impurity-discommensuration separation u_s. In the small-u_0 limit, this reduces to

$$E_{\rm mis}=2\pi\Delta u_0 e^{-|u_s|} . \quad (2.12)$$

The major difference between this expression and that found by solving the full sine-Gordon equation[10] is that $e^{-|u_s|}$ is replaced by $(2\cosh u_s)^{-1}$.

B. Modulus impurities

When $\Delta\equiv 0$ and β is nonuniform, the system contains elastic-modulus impurities [$\beta(u)\not\equiv\beta$], and the equilibrium displacement field satisfies $\phi_{uu}(u)-\beta(u)[\phi(u)\times(\mathrm{mod}\,2\pi)]=0$. Again, we consider a steplike impurity of length $2u_0$ [i.e., $\beta(u)=1$ for $|u|>u_0$, and $\beta(u)=\beta\neq 1$ for $|u|\le u_0$]. The interaction energy of a discommensuration with a modulus impurity can now be found by following the same procedure as for the misfit impurity. The main difference is that, by itself, the modulus impurity has no displacement field [i.e., one finds $\phi_{\rm mod}(u)\equiv 0$ and $H[\phi_{\rm mod}]=0$]. However, the calculation still proceeds as before to yield (for $|u_s|>u_0$)

$$E_{\rm mod}=\frac{\pi^2(\beta-1)\sinh(2\beta^{1/2}u_0)}{(\beta+1)\sinh(2\beta^{1/2}u_0)+2\beta^{1/2}\cosh(2\beta^{1/2}u_0)} \times e^{2(u_0-|u_s|)} . \quad (2.13)$$

Unlike the interaction potential between the discommensuration and the misfit impurity, the interaction potential between the discommensuration and the modulus impurity is not simply linear in the strength $\beta-1$ of the defect (although it does contain an overall factor of $\beta-1$). It does, however, show a similar exponential decay with separation. The dependence of the preexponential factor of Eq. (2.13) on the defect strength (i.e., on β) is shown in Fig. 3. In the small-u_0 limit, the interaction energy (2.13) reduces to

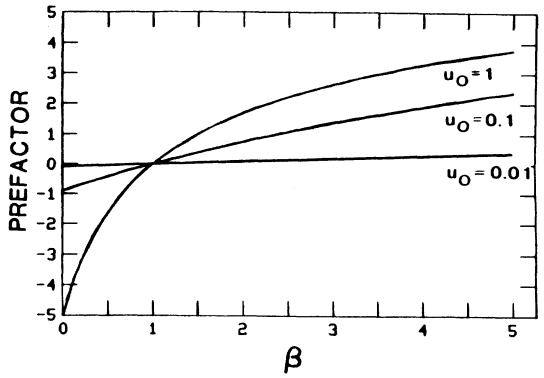

FIG. 3. Dependence of the preexponential factor in Eq. (2.13) on the defect strength for impurities of various sizes. The curves intersect at $\beta=1$, since this represents no defect, in which case $E_{\rm mod}=0$.

$$E_{\rm mod}=\pi^2(\beta-1)u_0 e^{-2|u_s|} , \quad (2.14)$$

which is simply linear in $\beta-1$.

III. THE STEADY-STATE IMPURITY CONCENTRATION PROFILE

We begin by assuming that the interaction potential between an impurity and a discommensuration depends on only their separation, and is independent of the velocity of the discommensuration. The chemical potential of the impurity is assumed to be given by[9,14]

$$\mu(x)=kT\ln C(x)+E(x) , \quad (3.1)$$

where C is the impurity concentration, kT is the thermal energy, and E is the impurity-discommensuration interaction potential. Note that, in Eq. (3.1), we have assumed that the impurity concentration is small (i.e., that it is consistent with Henry's law[14]). In the following discussion, we also assume that the discommensuration velocity is small compared with the smallest sound velocity (or any other limiting velocity), so that "relativistic" corrections can be ignored. The diffusion equation for the impurities may then be written as[9]

$$C_t=DC_{xx}+DE_xC_x/kT+DCE_{xx}/kT , \quad (3.2)$$

where D is the constant impurity diffusivity. In steady state, $C(x,t)$ depends only on $w=x-vt$ ($w=0$ is the position of the discommensuration), so that $C_t=-vC_w$ and $C_x=C_w$, and Eq. (3.2) becomes

$$C_{ww}+(v/D)C_w+(CE_w/kT)_w=0 . \quad (3.3)$$

Integrating Eq. (3.3) once and applying the appropriate boundary conditions far from the discommensuration [$E_w(\pm\infty)=0$, $C_w(\pm\infty)=0$, and $C(\pm\infty)=C_0$], we obtain the first-order differential equation

$$C_w+(v/D+E_w/kT)C=vC_0/D\ , \tag{3.4}$$

which is solved to yield

$$C(w)=(vC_0/D)\int_0^\infty e^{-vz/D}e^{-[E(w)-E(w-z)]/kT}dz\ . \tag{3.5}$$

A. General solution

To apply Eq. (3.5) to the impurity-discommensuration problem, we make use of the explicit forms for the interaction potential derived in Sec. II. The interaction potentials of both the misfit [Eqs. (2.11) and (2.12)] and modulus [Eqs. (2.13) and (2.14)] impurities have the same spatial dependence, which we write as

$$E(w)=E_0e^{-|w|/a}\ . \tag{3.6}$$

In this expression, a is the interatomic separation a_0, in the case of misfit impurities, and it is half this separation for the modulus impurities. E_0 depends on the strength of the impurity (Δ or $\beta-1$) and can, in principle, be either positive or negative, depending on the nature of the impurity-discommensuration interaction. Inserting this expression for the interaction potential into Eq. (3.5) and letting $\rho=va/D$, $\sigma=E_0/kT$, and $u=w/a$, we find

$$C(u)=\rho C_0e^{-\rho u}e^{-\sigma e^{-|u|}}\int_{-u}^\infty e^{-\rho z}e^{\sigma e^{-|z|}}dz\ . \tag{3.7}$$

Performing the integration gives

$$C(u)=\begin{cases}C_0\Gamma(\rho+1)e^{-\sigma e^{-|u|}}\gamma^*(\rho,-\sigma e^{-|u|}), & u\le 0\\ C_0e^{-\sigma e^{-u}}\{\Gamma(-\rho+1)\gamma^*(-\rho,-\sigma e^{-u})+e^{-\rho u}[\Gamma(\rho+1)\gamma^*(\rho,-\sigma)-\Gamma(-\rho+1)\gamma^*(-\rho,-\sigma)]\}, & u>0\ ,\end{cases} \tag{3.8}$$

where $\Gamma(a)$ is the standard (complete) γ function, and

$$\gamma^*(a,x)=\frac{1}{\Gamma(a)}\int_0^1 z^{a-1}e^{-xz}dz \tag{3.9}$$

is the modified, incomplete γ function, which is discussed in the Appendix.

In Figs. 4 and 5, we plot C as a function of u for a number of choices of the discommensuration velocity ($\rho=va/D$) and impurity strength ($\sigma=E_0/kT$). These figures show that, for an attractive interaction ($\sigma<0$), the concentration profile is peaked at the discommensuration (i.e., at $u=0$), while, for a repulsive interaction ($\sigma>0$), there are dips in the concentration profile, instead of peaks. The size of the peak or dip decreases with increas-

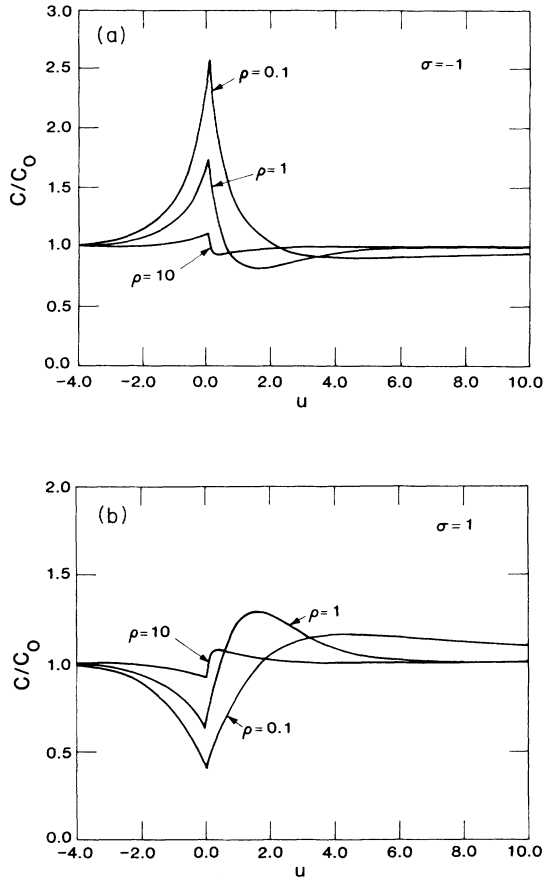

FIG. 4. Impurity concentration as a function of position for various discommensuration velocities. In each case, the discommensuration is at $u=0$ and is moving to the right. Cases (a) and (b) are for attractive and repulsive impurity-discommensuration interactions, respectively.

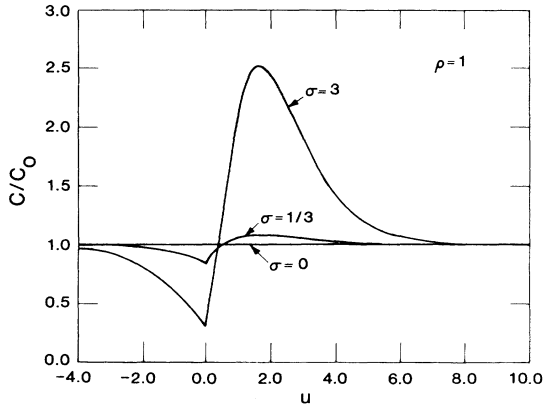

FIG. 5. Impurity concentration profile for various (repulsive) impurity-discommensuration interaction strengths. Again, the discommensuration is at $u=0$ and moving to the right. In particular, note the large impurity concentration piled up in front of the moving discommensuration, causing the net excess concentration to be positive, even though the impurity-discommensuration interaction is repulsive.

ing discommensuration velocity, decreasing diffusivity, and/or decreasing interaction strength. Comparison of Figs. 4(a) and 4(b) shows that, for the same value of $|\sigma|$, the peak for $\sigma<0$ has greater amplitude than the dip for $\sigma>0$ [see the discussion following Eq. (3.13)].

The concentration profile is not symmetric with respect to the discommensuration position [i.e., $C(u)\neq C(-u)$]. This asymmetry becomes more pronounced with increasing ρ (i.e., increasing discommensuration velocity or decreasing impurity diffusivity). At sufficiently high velocity (low diffusivity), the concentration profile begins to resemble a shock, or concentration discontinuity, at the discommensuration. Even so, $C(u)$ always remains continuous at $u=0$, although its derivative does not. However, this discontinuity in the derivative is traceable to the same discontinuity in the derivative of the potential $E(w)$ of Eq. (3.6), and, thus, it need not be physical (such a discontinuity does not occur in the solution when the full sine-Gordon equation is employed). Finally, note that, in Eq. (3.8), although $\Gamma(-\rho+1)$ diverges at positive, integer values of ρ, the full expression remains finite and continuous everywhere.

B. Limiting cases

For the case $\rho=0$ (zero discommensuration velocity or infinite diffusivity), the concentration profile reduces to

$$C(u;\rho=0)=C_0\exp(-\sigma e^{-|u|}) . \tag{3.10}$$

This is the expected, equilibrium, impurity concentration profile (for small impurity concentration) about a static discommensuration. For $\rho>0$ and $|u|\gg 1$, Eq. (3.8) reduces to

$$C(u)=\begin{cases} C_0\left(1-\dfrac{\sigma}{\rho+1}e^{-|u|}\right), & u<0 \\ C_0\left\{1+\dfrac{\sigma}{\rho-1}e^{-u}+e^{-\rho u}[\Gamma(\rho+1)\gamma^*(\rho,-\sigma)-\Gamma(-\rho+1)\gamma^*(-\rho,-\sigma)]\right\}, & u>0 \text{ and } \rho\neq 1 \\ C_0\{1+e^{-u}[\sigma(u-\gamma)+\gamma^*(1,-\sigma)-\gamma_1^*(-1,-\sigma)]\}, & u>0 \text{ and } \rho=1 , \end{cases} \tag{3.11}$$

where γ is Euler's constant, and $\gamma_1^*(a,x)=\partial\gamma^*(a,x)/\partial a$ is discussed in the Appendix. Also, note that, in the middle expression, only the dominant exponential (e^{-u}, for $\rho>1$, or $e^{-\rho u}$, for $\rho<1$) is significant. From these asymptotic relations, we see that, behind the moving discommensuration, the concentration profile decays exponentially as $e^{-|u|}$, while, ahead of the discommensuration, it decays as $e^{-\rho u}$, for $\rho<1$, and as e^{-u}, for $\rho\geq 1$.

On the other hand, for $|u|\ll 1$, the concentration profile is given by (for all ρ)

$$C(u)=C_0\Gamma(\rho+1)e^{-\sigma}[\gamma^*(\rho,-\sigma)+\sigma|u|\gamma^*(\rho,-\sigma) +\rho\sigma u\gamma^*(\rho+1,-\sigma)] . \tag{3.12}$$

At the center of the discommensuration, the impurity concentration is given by

$$C(u=0)=C_0\Gamma(\rho+1)e^{-\sigma}\gamma^*(\rho,-\sigma) . \tag{3.13}$$

Because of the factor $e^{-\sigma}$, the peaks in the impurity concentration for $\sigma<0$ are larger than are the dips for $\sigma>0$. The third term in Eq. (3.12) is the source of the asymmetry about the moving discommensuration at $u=0$. Hence, it is this term which is responsible for the formation of the shocklike profile in Fig. 4. Examining this term, we see that the asymmetry vanishes for $\rho=0$, and it increases as ρ increases.

Finally, for $\rho\gg 1$ (i.e., $D\ll va$), we have

$$C(u)=\begin{cases} C_0\left[1-\dfrac{\sigma}{\rho}e^{-|u|}\right], & u\leq 0 \\ C_0\left[1+\dfrac{\sigma}{\rho}e^{-u}-\dfrac{2\sigma}{\rho}e^{\sigma}e^{-\rho u}e^{-\sigma e^{-u}}\right], & u>0 , \end{cases} \tag{3.14}$$

where the final term in the second expression is unimportant, except very near the discommensuration ($u=0$). From this expression, we see that, as ρ increases, the deviation of the concentration $C(u)$ from a uniform value C_0 vanishes as $|C(u)-C_0|/C_0=(|\sigma|/\rho)e^{-|u|}$.

C. Excess concentration

We conclude this section with a discussion of the excess concentration carried along with the moving discommensuration:

$$\Delta C=\int_{-\infty}^{\infty}[C(u)-C_0]du . \tag{3.15}$$

Using Eq. (3.8), this becomes

$$\Delta C=2C_0[\Gamma(\rho+1)]^2 \times\int_0^{|\sigma|} z\gamma^*(\rho+1,z)\gamma^*(\rho+1,-z)dz \tag{3.16}$$

[in deriving Eq. (3.16) from Eq. (3.15), we have made repeated use of the recursion relations for $\gamma^*(a,x)$ which are discussed in the Appendix]. From Eq. (3.16), we see that the excess concentration ΔC depends only on the strength $|\sigma|$ of the impurity-discommensuration interaction, and not on its sign. In particular, ΔC is *always* positive.

Near the discommensuration (on the order of a lattice spacing) is a "core" excess concentration which is positive (negative) for an attractive (repulsive) interaction. However, in front of the discommensuration is a long "tail" of the opposite sign (cf. Figs. 4 and 5). For an attractive interaction, the discommensuration drags an excess impurity concentration along with it, leading to a large (positive) core and a small (negative) tail. On the other hand, for a

repulsive interaction, the discommensuration piles up an excess concentration in front of it, leading to a large (positive) tail and a small (negative) core. In either case, the *net* excess concentration ΔC is positive.[15] Consequently, one cannot determine the sign of the impurity-discommensuration interaction from the sign of the excess impurity concentration about a moving discommensuration. However, note that the tail is a *dynamic* effect and vanishes for a *static* discommensuration [cf. Eq. (3.10)]. Thus, for a static, equilibrium discommensuration, such a sign determination may be possible.

Finally, we note that the *total* excess concentration must be zero (because of mass conservation). The quantity ΔC in Eq. (3.15) is the excess concentration moving with the discommensuration. In addition, there is a *stationary* deficit $-\Delta C$ left behind during the transient acceleration of the discommensuration. When steady state has been reached, this deficit has become localized at $u=-\infty$ in the moving frame of reference. For a *finite* system, the steady-state profile is never *completely* attained, and this deficit is present at a finite distance behind the discommensuration. In this case, whether or not the two contributions ΔC and $-\Delta C$ can be isolated depends on the probe size.

IV. IMPURITY DRAG FORCE ON THE DISCOMMENSURATIONS

Because of the impurity-discommensuration interaction, a discommensuration feels a drag force arising from the impurity concentration profile about it. The force from a single impurity is $-dE(w)/dw$, so the total drag force is given by

$$F_{\text{drag}}=\int_{-\infty}^{\infty} C(w)\left[-\frac{dE(w)}{dw}\right]dw\ , \tag{4.1}$$

which, for the potential (3.6), becomes (again using $u=w/a$)

$$F_{\text{drag}}=E_0\int_0^{\infty} e^{-u}[C(u)-C(-u)]du\ . \tag{4.2}$$

Note that, in the remainder of this paper, we take the concentration to be the number of impurities per unit *length* along the direction of motion of the discommensuration. For the steady-state concentration profile (3.8), this drag force is found to be

$$F_{\text{drag}}=2C_0\rho kT[\Gamma(\rho+1)]^2 \times\int_0^{|\sigma|} z\gamma^*(\rho+1,z)\gamma^*(\rho+1,-z)dz \tag{4.3}$$

[in deriving Eq. (4.3) from Eq. (4.2), we have again made repeated use of the recursion relations for $\gamma^*(a,x)$ which are discussed in the Appendix]. From this expression, we see that the drag force depends only on the strength $|\sigma|$ of the impurity-discommensuration interaction, and not on its sign.

Notice that the above expression (4.3) for the drag force F_{drag} is very similar to the expression (3.16) for the excess concentration ΔC. This similarity is not accidental. From Eq. (3.4), we have

$$C-C_0=-DC_w/v-DCE_w/vkT\ . \tag{4.4}$$

Equation (3.15) then yields [since $u=w/a$, $\rho=va/D$, and $C(\pm\infty)=C_0$]

$$\Delta C=-(1/\rho kT)\int_{-\infty}^{\infty} CE_w dw=F_{\text{drag}}/\rho kT\ , \tag{4.5}$$

where we have made use of Eq. (4.1). Thus, the excess concentration and the drag force are related by the simple expression (4.5).

A. Limiting cases

For $\rho\gg 1$ ($D\ll va$), Eq. (4.3) reduces to

$$F_{\text{drag}}=C_0\sigma^2 kT/\rho\ , \tag{4.6}$$

while, for $\rho\ll 1$ (low velocity or high diffusivity), it becomes

$$F_{\text{drag}}=8C_0\rho kT\int_0^{2|\sigma|}\frac{\sinh^2 z}{z}dz$$

$$=4C_0\rho kT(\text{chi}\,|\sigma|-\ln|\sigma|-\gamma)\ , \tag{4.7}$$

where chi(z) is the hyperbolic-cosine-integral function,[16] and γ is Euler's constant. Both of these results are in agreement with those of Cahn[9] [see his Eqs. (12) and (15)].

For low discommensuration velocity or fast impurity diffusion (i.e., for small ρ), the impurity concentration profile is nearly symmetric about the discommensuration [for $\rho=0$, it is perfectly symmetric, as shown by Eq. (3.10)]. Since the drag force F_{drag} scales with the asymmetry $C(u)-C(-u)$ of the impurity concentration profile [cf. Eq. (4.2)], then it must vanish as $\rho\to 0$, as verified by Eq. (4.7). As ρ increases from $\rho=0$, the asymmetry in the concentration profile becomes more pronounced, leading to an increase in the drag force. For large ρ, the concentration profile continues to increase its asymmetry, becoming shocklike; however, its peak amplitude is now decreasing. As $\rho\to\infty$, this amplitude vanishes, and the concentration becomes uniform (and, thus, symmetric), since the impurities can no longer adjust to the moving discommensuration (because $D\ll va$). Hence, as $\rho\to\infty$, F_{drag} must again vanish, as verified by Eq. (4.6). Thus, we see that F_{drag} begins increasing linearly with ρ, after which it peaks and then decreases as $1/\rho$.

For small interaction strength $|\sigma|\ll 1$, Eq. (4.3) reduces to

$$F_{\text{drag}}=C_0\rho\sigma^2 kT/(\rho+1)^2\propto\rho/(\rho+1)^2\ . \tag{4.8}$$

This should be compared with the expression $\rho/(\rho^2+1)$ assumed by Cahn,[9] for a triangular-well potential, to fit the same asymptotic behaviors ρ and $1/\rho$ for $\rho\ll 1$ and $\rho\gg 1$, respectively. The limit of large interaction strength $|\sigma|\gg 1$ is much more complicated, and the resulting expression for F_{drag} simplifies only in the following two cases (both for $|\sigma|\gg 1$):

$$F_{\text{drag}}=\begin{cases}2C_0\rho kT\Gamma(\rho+1)\,|\sigma|^{-(\rho+1)}e^{|\sigma|}, & \rho\ll|\sigma| \\ C_0\sigma^2 kT/\rho, & \rho\gg|\sigma|\end{cases} \tag{4.9}$$

(for $\rho\cong|\sigma|$, neither expression is valid, and no simple expression can be found). Examining Eqs. (4.8) and (4.9), we find that the peak ρ^* in F_{drag} begins at $\rho^*=1$, for

$|\sigma| \ll 1$, decreases as the interaction strength $|\sigma|$ increases, and approaches zero as $\rho^* = 1/\ln|\sigma|$, for $|\sigma| \gg 1$.

B. Dissipation theorem

We conclude this section with a self-consistency check. For steady-state, viscous-drag problems of the type considered here, the drag force can be found from a dissipation theorem.[17] In one dimension (as is the case here), the dissipation theorem yields

$$F_{\text{drag}} = \frac{kT}{Dv} \int_{-\infty}^{\infty} [J^2(x)/C(x)]dx \ , \tag{4.10}$$

where $J(x)$ is the concentration flux (in the stationary reference frame):

$$C_t = -J_x \ . \tag{4.11}$$

From Eq. (3.2), we see that

$$J = -DC_x - DCE_x/kT \ . \tag{4.12}$$

Furthermore, from Eq. (4.4), we see that this may be rewritten as

$$J = v(C - C_0) \ . \tag{4.13}$$

In the high-velocity limit, we have $C \cong C_0$, and the first term in Eq. (4.12) becomes negligible, yielding $J \cong -DCE_x/kT$. Inserting these expressions into Eq. (4.10), we do indeed recover the high-velocity drag force (4.6). On the other hand, in the low-velocity limit, it is convenient to use the simpler expression (4.13). Inserting this into Eq. (4.10) and using the low-velocity concentration profile (3.10), we also recover the low-velocity drag force (4.7).

Finally, we wish to point out that the previous applications of this dissipation-theorem approach[17] have involved very simple forms of the interaction potential $E(x)$ (e.g., square wells). Here, however, we have verified this approach for a much more realistic potential, which has provided a more stringent test of the concept.

V. DISCOMMENSURATION VELOCITY VERSUS APPLIED FIELD

In the absence of impurities, applying an external field to a system causes the discommensurations to feel an applied force F_{app}, and, thus, to move at some velocity $v_0(F_{\text{app}})$. The detailed form of the function $v_0(F)$ depends on the physical nature of the discommensuration (e.g., charge-density wave, ferroelectric domain wall, grain boundary, etc.). However, certain qualitative features are common to most types of discommensuration. At low fields, $v_0(F)$ is generally linear,[18] being given by $v_0 = MF$, where M is the mobility of the discommensurations (which can vary widely among different systems). On the other hand, at large fields, $v_0(F)$ generally saturates at some limiting velocity v_∞, which is usually the smallest sound velocity (or the velocity of some other excitation in the system).

When impurities are present, the discommensurations no longer feel just the applied force F_{app}. Instead they feel the total force $F_{\text{tot}} = F_{\text{app}} - F_{\text{drag}}$, where F_{drag} is the drag force due to the impurities (which was discussed in Sec. IV). Thus, in the presence of impurities, the resulting discommensuration velocity is $v(F_{\text{app}}) = v_0(F_{\text{tot}}) = v_0(F_{\text{app}} - F_{\text{drag}})$, with $v_0(F)$ being the force-velocity relationship, discussed above, in the absence of the impurities. Since F_{drag} depends on the resulting velocity $v(F_{\text{app}})$, then this new (self-consistent) force-velocity relationship $v(F)$ may be much more complicated than that for the impurity-free case. In particular, in the presence of impurities, $v(F)$ may exhibit hysteresis.

For the form of $F_{\text{drag}}(\rho)$ given by Eq. (4.3), the force-velocity relationship in the presence of impurities has one of the two qualitative forms shown in Fig. 6. For a system with the relationship shown in Fig. 6(b), hysteresis can occur. As the applied force F_{app} is increased from zero, the resulting (dimensionless) velocity $\rho(F_{\text{app}})$ increases linearly with F_{app} (but with a smaller slope than in the impurity-free case). However, as F_{app} continues increasing, $\rho(F_{\text{app}})$ begins increasing faster than linearly. Finally, at $F_{\text{app}} = F_+$, the velocity reaches $\rho = \rho_+$ and then jumps discontinuously[19] to $\rho = \tilde{\rho}_+ > \rho_+$. If the force continues to increase, the velocity eventually saturates at $\rho = \rho_\infty$. If the applied force is now decreased, the velocity decreases continuously below $\rho = \tilde{\rho}_+$, and, depending on the particular system, this decrease will generally become linear in F_{app}. At $F_{\text{app}} = F_- < F_+$, the velocity reaches $\rho = \rho_- < \tilde{\rho}_+$ and then jumps discontinuously[19] to $\rho = \tilde{\rho}_- < \rho_-$. Finally, as the force continues decreasing to zero, so does the velocity.

Since the qualitative form of the impurity-free force-velocity relationship is insensitive to the specific nature of the discommensuration, we return to the case of a discommensuration governed by the sine-Gordon equation. For such a discommensuration, the impurity-free force-velocity relationship is given by[20]

$$v_0(F) = v_\infty [1 + (F_0/F)^2]^{-1/2} \ , \tag{5.1}$$

where v_∞ is the saturation velocity, and $F_0 = 4\alpha/\pi$, with α the damping coefficient in the dimensionless sine-Gordon equation. Using the relationship $v(F_{\text{app}}) = v_0(F_{\text{tot}})$ and switching to the dimensionless velocity $\rho = va/D$ yields the desired force-velocity relationship in the presence of the impurities:

$$F_{\text{app}} = F_{\text{drag}}(\rho) + F_0[(\rho_\infty/\rho)^2 - 1]^{-1/2} \ , \tag{5.2}$$

where $\rho_\infty = v_\infty a/D$ and $F_{\text{drag}}(\rho)$ is discussed in Sec. IV. For all of our quantitative results, we assume that $\rho_\infty \gg 1$, which amounts to assuming that the impurities diffuse slowly compared to v_∞. At this point, we reiterate that, although the *quantitative* results in this section are valid only for discommensurations governed by the sine-Gordon equation, the *qualitative* features of these results are valid for most types of discommensurations [specifically, those whose impurity-free force-velocity relationships $v_0(F)$ begin linearly and saturate at large F].

If hysteresis exists in a given system, then the force-velocity relationship consists of two (overlapping) stable branches [cf. Fig. 6(b)]. These two branches correspond to the two terms in Eq. (5.2). For most physical systems (including all of the systems considered in this paper),

these two branches (terms) have little effect on each other (except, of course, near the transition region). Thus, the lower branch ($F_{app} < F_+$) is the impurity-dominated motion given by $F_{app} \cong F_{drag}(\rho)$, and the upper branch ($F_{app} > F_-$) is the impurity-free motion $F_{app} \cong F_0[(\rho_\infty/\rho)^2 - 1]^{-1/2}$. As a result, the hysteresis amounts to sudden changes between impurity-dominated and impurity-free motion as the applied field is varied. In particular, for fields above the hysteresis threshold (i.e., for $F_{app} > F_+$), the motion of a discommensuration is the same as for an impurity-free system (since it has broken free of the impurities).

Whether or not a given system exhibits hysteresis depends on the values of the physical parameters specifying that system. For a system with the sine-Gordon force-velocity relationship (5.2), these parameters are F_0, ρ_∞, C_0, σ, and kT. Using the explicit expression (5.2), we can find the conditions for the onset of hysteresis, as well as explicit expressions for the quantities characterizing the hysteresis (i.e., F_+, F_-, ρ_+, $\tilde{\rho}_+$, ρ_-, and $\tilde{\rho}_-$). In this section, we summarize our analytic results. In Sec. VII, we apply these results to three physical systems: charge-density waves, ferroelectric domain walls, and grain boundaries.

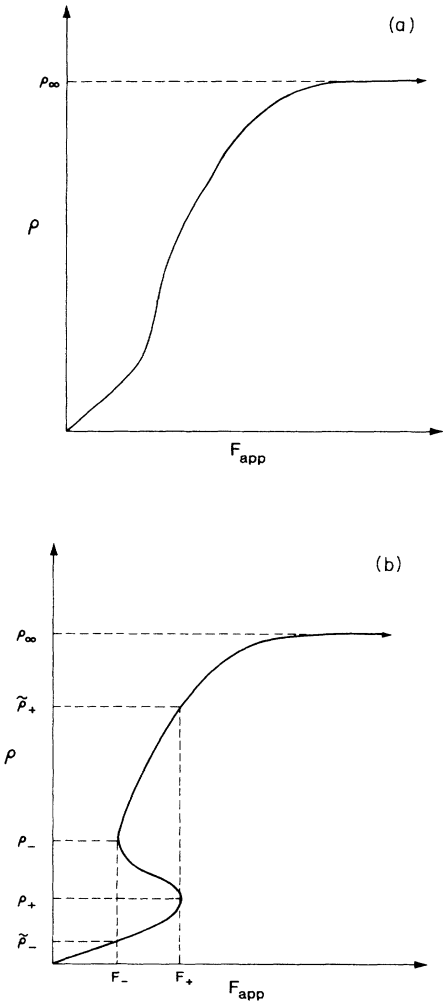

FIG. 6. Qualitative forms of the dependence of the discommensuration velocity on the applied force. This force-velocity relationship makes a transition from an impurity-dominated regime, at low forces, to an impurity-free regime, at high forces (the latter behavior being the same as for an impurity-free material). This transition can be either (a) gradual or (b) hysteretic. In either case, the velocity must saturate at high fields (to, for example, the smallest sound velocity).

A. Weak-interaction limit

We begin with the limit of small impurity-discommensuration interaction strength $|\sigma| \ll 1$, in which case $F_{drag}(\rho)$ is given by the simple expression (4.8). An example of a system with $|\sigma| \ll 1$ is provided by charge-density-wave materials. For such materials, the impurity-discommensuration interaction strength $|E_0|$ is typically on the order of 1—10 meV, which yields $|\sigma| = 0.04 - 0.4$ (at room temperature). In this weak-interaction limit, whether or not hysteresis occurs depends *only* on the combination of parameters

$$\lambda = C_0 \rho_\infty \sigma^2 kT/F_0 \ . \tag{5.3}$$

The critical value of this parameter (i.e., where $F_+ = F_-$) is $\lambda_c = 27$, and hysteresis does (does not) exist for $\lambda > \lambda_c$ ($\lambda < \lambda_c$).

This criterion may become more clear if the expression (5.3) for λ is rewritten in terms of the mobility. For small forces F (or, equivalently, for small velocities), Eq. (5.1) becomes $v_0(F) = (v_\infty/F_0)F = MF$, which shows that the mobility is given by

$$M = v_\infty/F_0 = \rho_\infty D/F_0 a \ . \tag{5.4}$$

Thus, Eq. (5.3) can be rewritten as

$$\lambda = MC_0 a \sigma^2 kT/D \ . \tag{5.5}$$

Since $C_0 a$ is the *fractional* concentration of impurities, then one generally has $C_0 a \ll 1$ (in addition to the condition $|\sigma| \ll 1$). Thus, in the weak-interaction limit, hysteresis can occur only in systems with high mobility or low diffusivity. To examine the temperature dependence of λ, we must realize that M and D generally have the temperature dependences (with $Q_M, Q_D > 0$):

$$M = M_0 e^{-Q_M/kT} \ , \tag{5.6}$$

$$D = D_0 e^{-Q_D/kT} \ , \tag{5.7}$$

which yields (since $\sigma = E_0/kT$)

$$\lambda \propto T^{-1} e^{(Q_D - Q_M)/kT} \ . \tag{5.8}$$

Thus, we see that λ is *very* sensitive to temperature. In particular, hysteresis may appear or disappear as the temperature is varied (whether λ increases or decreases as the temperature increases depends on whether Q_M is larger or smaller than Q_D, which depends on the system studied).

We now summarize our results for the quantities F_+, F_-, ρ_+, $\tilde{\rho}_+$, ρ_-, and $\tilde{\rho}_-$ (again, for $|\sigma| \ll 1 \ll \rho_\infty$). In general, we have

$$\rho_+ = -1+2(\tfrac{1}{3}\lambda)^{1/2}\cos\{\tfrac{1}{3}\pi+\tfrac{1}{3}\cos^{-1}[(\lambda_c/\lambda)^{1/2}]\}\ , \tag{5.9}$$

$$\rho_- = \begin{cases} -1+2(\tfrac{1}{3}\lambda)^{1/2}\cos\{\tfrac{1}{3}\pi-\tfrac{1}{3}\cos^{-1}[(\lambda_c/\lambda)^{1/2}]\}, & \lambda^{1/2}\ll\rho_\infty \\ (\rho_\infty^3/\lambda\lambda_c^{1/2})\{-1+2\cos[\tfrac{1}{3}\cos^{-1}(\lambda^2\lambda_c/2\rho_\infty^4-1)]\}^{3/2}, & \lambda^{1/2}\gg 1 \end{cases} \tag{5.10}$$

$$F_+ = (F_0/\rho_\infty)(1+\tfrac{3}{4}\sec^2\{\tfrac{1}{3}\pi+\tfrac{1}{3}\cos^{-1}[(\lambda_c/\lambda)^{1/2}]\})(-1+2(\tfrac{1}{3}\lambda)^{1/2}\cos\{\tfrac{1}{3}\pi+\tfrac{1}{3}\cos^{-1}[(\lambda_c/\lambda)^{1/2}]\})\ , \tag{5.11}$$

$$F_- = \begin{cases} (F_0/\rho_\infty)(1+\tfrac{3}{4}\sec^2\{\tfrac{1}{3}\pi-\tfrac{1}{3}\cos^{-1}[(\lambda_c/\lambda)^{1/2}]\})(-1+2(\tfrac{1}{3}\lambda)^{1/2}\cos\{\tfrac{1}{3}\pi-\tfrac{1}{3}\cos^{-1}[(\lambda_c/\lambda)^{1/2}]\}), & \lambda^{1/2}\ll\rho_\infty \\ F_0[(\lambda^2\lambda_c^{1/2}/\rho_\infty^4)\{-1+2\cos[\tfrac{1}{3}\cos^{-1}(\lambda^2\lambda_c/2\rho_\infty^4-1)]\}^{-3/2} & \\ \quad +((\lambda^2\lambda_c/\rho_\infty^4)\{-1+2\cos[\tfrac{1}{3}\cos^{-1}(\lambda^2\lambda_c/2\rho_\infty^4-1)]\}^{-3}-1)^{-1/2}], & \lambda^{1/2}\gg 1\ . \end{cases} \tag{5.12}$$

Analytic results for $\tilde{\rho}_+$ and $\tilde{\rho}_-$ can also be found, but these expressions are even more involved and less illuminating. In Eqs. (5.10) and (5.12), note that the regions $\lambda^{1/2}\ll\rho_\infty$ and $\lambda^{1/2}\gg 1$ overlap (since $\rho_\infty\gg 1$), so that at least one of these two cases is *always* valid. Also, for $\lambda^{1/2}\gg 1$, the identity $\cos(\frac{1}{3}\cos^{-1}x)=\cosh(\frac{1}{3}\cosh^{-1}x)$ is useful when the argument x exceeds 1.

While the expressions (5.9)—(5.12) are general and exact, they are not very illuminating. Consequently, we also list the following special cases:

$$\rho_+ = \begin{cases} 2, & \lambda=\lambda_c \\ 1, & \lambda^{1/2}\gg\lambda_c^{1/2} \end{cases} \tag{5.13}$$

$$\rho_- = \begin{cases} 2, & \lambda=\lambda_c \\ \lambda^{1/2}, & \lambda_c^{1/2}\ll\lambda^{1/2}\ll\rho_\infty \\ \rho_\infty, & \lambda^{2/3}\gg\rho_\infty^{4/3}/3 \end{cases} \tag{5.14}$$

$$\tilde{\rho}_+ = \begin{cases} 2, & \lambda=\lambda_c \\ \lambda/4, & \lambda^{1/2}\gg\lambda_c^{1/2}, \text{ and } \lambda\ll 4\rho_\infty \\ \rho_\infty, & \lambda\gg 4\rho_\infty \end{cases} \tag{5.15}$$

$$\tilde{\rho}_- = \begin{cases} 2, & \lambda=\lambda_c \\ 2\lambda^{-1/2}, & \lambda_c^{1/2}\ll\lambda^{1/2}\ll\rho_\infty \\ 1/\rho_\infty, & \lambda^{2/3}\gg\rho_\infty^{4/3}/3 \end{cases} \tag{5.16}$$

$$F_+ = \begin{cases} 8F_0/\rho_\infty, & \lambda=\lambda_c \\ \lambda F_0/4\rho_\infty, & \lambda^{1/2}\gg\lambda_c^{1/2} \end{cases} \tag{5.17}$$

$$F_- = \begin{cases} 8F_0/\rho_\infty, & \lambda=\lambda_c \\ 2\lambda^{1/2}F_0/\rho_\infty, & \lambda^{1/2}\gg\lambda_c^{1/2}, \text{ and } \lambda\ll 4\rho_\infty \\ \lambda F_0/\rho_\infty^2, & \lambda\gg 4\rho_\infty\ . \end{cases} \tag{5.18}$$

B. Strong-interaction limit

Next, we consider the opposite limit: that of large impurity-discommensuration interaction strength $|\sigma|\gg 1$. As mentioned in Sec. IV, $F_{\rm drag}(\rho)$ is much less tractable in this limit, simplifying only in the two extremes given in Eq. (4.9). Furthermore, the first of these two expressions is by no means simple. Nonetheless, we can still extract a considerable amount of useful information in this limit. In addition, this limit is physically interesting: for both ferroelectric domain walls and grain boundaries, the impurity-discommensuration interaction strength $|E_0|$ is typically on the order of 0.1—1 eV, which yields $|\sigma|=4-40$ (again at room temperature).

For $\rho_\infty, |\sigma|\gg 1$, whether or not hysteresis occurs again depends on only a single parameter:

$$\Lambda = C_0\rho_\infty kTe^{|\sigma|}/F_0|\sigma|\ . \tag{5.19}$$

The critical value of this parameter is $\Lambda_c=e^2/2$ (everywhere in this paper, e denotes the base of the natural logarithm, not the electronic charge), and we have that hysteresis does (does not) exist for $\Lambda>\Lambda_c$ ($\Lambda<\Lambda_c$). As before, this expression can be rewritten in terms of the mobility:

$$\Lambda = MC_0akTe^{|\sigma|}/D|\sigma|\ . \tag{5.20}$$

Thus, in the strong-interaction limit $|\sigma|\gg 1$, hysteresis should be quite common, occurring unless the system exhibits low mobility or high diffusivity. From Eqs. (5.6) and (5.7) and $\sigma=E_0/kT$, we see that Λ has the temperature dependence

$$\Lambda \propto T^2 e^{(Q_D-Q_M+|E_0|)/kT}\ . \tag{5.21}$$

Thus, as before, Λ is *very* sensitive to temperature, and hysteresis may appear or disappear as the temperature is varied. Also, Λ may either increase or decrease as the temperature increases, depending on the sign of $Q_D-Q_M+|E_0|$.

In the strong-interaction limit, the general expressions for F_+, F_-, ρ_+, $\tilde{\rho}_+$, ρ_-, and $\tilde{\rho}_-$ are much more involved than those in the weak-interaction limit. Consequently, we give results only for some special cases. In order to state these results more clearly, we list some of these cases below.

Case I:

$$\ln|\sigma| \ll \ln\Lambda < \rho_\infty \ln|\sigma| \quad \text{and} \quad \ln(\ln\Lambda/\ln|\sigma|)\ll\ln|\sigma|\ .$$

Case IIa:

$$\rho_\infty \ll |\sigma| \quad \text{and} \quad \Lambda^{2/3} \gg (1/4\pi^{1/3}) \left[\left[\frac{e|\sigma|}{\rho_\infty} \right]^{\rho_\infty} \Big/ \ln \left[\frac{|\sigma|}{\rho_\infty} \right] \right]^{2/3} .$$

Case IIb:

$$\rho_\infty \ll |\sigma| \quad \text{and} \quad \Lambda^{2/3} \gg (1/2\pi^{1/3}) \left[\left[\frac{e|\sigma|}{\rho_\infty} \right]^{2\rho_\infty} \times \ln \left[\frac{|\sigma|}{\rho_\infty} \right] \right]^{1/3} .$$

Case III:

$$\rho_\infty \gg |\sigma|, \quad \Lambda^{1/2} \gg |\sigma|^{-1/2} e^{|\sigma|/2},$$

and

$$\Lambda \ll 2\rho_\infty^2 e^{|\sigma|}/(3\sqrt{3}|\sigma|^3) .$$

Case IV:

$$\rho_\infty \gg |\sigma| \quad \text{and} \quad \Lambda^{2/3} \gg \sigma^{-2} \rho_\infty^{4/3} e^{2|\sigma|/3} .$$

These four cases are given in order of increasing Λ. Case I corresponds to the minimum ρ_- occurring well between $\rho=1$ and $\rho=|\sigma|$, where F_{drag} is decreasing rapidly, but before saturation at ρ_∞ (cf. Fig. 6). Cases II correspond to ρ_- being near saturation at ρ_∞ when saturation occurs before $\rho=|\sigma|$ (cases IIa and IIb are *slightly* different forms of the same condition, these two forms being appropriate for the evaluations of ρ_- and F_-, respectively). Case III corresponds to ρ_- occurring well beyond $|\sigma|$, but before saturation. Finally, case IV corresponds to ρ_- occurring well beyond $|\sigma|$ and near saturation.

Using the above case labels, we have the following results (again, for $\rho_\infty, |\sigma| \gg 1$):

$$\rho_+ = \begin{cases} 2/\ln|\sigma|, & \Lambda = \Lambda_c \\ 1/\ln|\sigma|, & \Lambda \gg \Lambda_c/e \end{cases} \tag{5.22}$$

$$\rho_- = \begin{cases} 2/\ln|\sigma|, & \Lambda = \Lambda_c \\ \ln\Lambda/\ln|\sigma|, & \text{case I} \\ \rho_\infty, & \text{case IIa} \\ \Lambda^{1/2}|\sigma|^{3/2} e^{-|\sigma|/2}, & \text{case III} \\ \rho_\infty, & \text{case IV} \end{cases} \tag{5.23}$$

$$\tilde{\rho}_+ = \begin{cases} 2/\ln|\sigma|, & \Lambda = \Lambda_c \\ \rho_\infty [1+(e\rho_\infty \ln|\sigma|/2\Lambda)^2]^{-1/2}, & \Lambda \gg \Lambda_c/e \end{cases} \tag{5.24}$$

$$\tilde{\rho}_- = \begin{cases} 2/\ln|\sigma|, & \Lambda = \Lambda_c \\ \rho_\infty F_-/2\Lambda F_0, & \ln 2\Lambda \gg 1 \end{cases} \tag{5.25}$$

$$F_+ = \begin{cases} 4F_0/(\rho_\infty \ln|\sigma|), & \Lambda = \Lambda_c \\ 2\Lambda F_0/(e\rho_\infty \ln|\sigma|), & \Lambda \gg \Lambda_c/e \end{cases} \tag{5.26}$$

$$F_- = \begin{cases} 4F_0/(\rho_\infty \ln|\sigma|), & \Lambda = \Lambda_c \\ [F_0 \ln\Lambda/(\rho_\infty \ln|\sigma|)]\{1-[\ln\Lambda/(\rho_\infty \ln|\sigma|)]^2\}^{-1/2}, & \text{case I} \\ 2\Lambda F_0 (2\pi\rho_\infty)^{1/2} (\rho_\infty/e|\sigma|)^{\rho_\infty}, & \text{case IIb} \\ (2\Lambda^{1/2} F_0 |\sigma|^{3/2}/\rho_\infty) e^{-|\sigma|/2}, & \text{case III} \\ (\Lambda F_0 |\sigma|^3/\rho_\infty^2) e^{-|\sigma|}, & \text{case IV} . \end{cases} \tag{5.27}$$

Note that, for all of the cases I–IV, we have $\ln 2\Lambda \gg 1$. Thus, in cases I, IIb, III, and IV, $\tilde{\rho}_-$ is given by the second expression in Eq. (5.25) with the appropriate expression for F_- from Eq. (5.27). In addition, we have one additional special case. For $\ln 2\Lambda \ll \ln|\sigma|$, letting η be the larger root of

$$e^\eta = 2\Lambda(\eta - 1) \tag{5.28}$$

(i.e., the root satisfying $\eta \geq 2$) yields

$$\rho_- = \eta/\ln|\sigma| , \tag{5.29}$$

$$F_- = F_0 \eta^2/[\rho_\infty(\eta-1)\ln|\sigma|] . \tag{5.30}$$

VI. STATIC-IMPURITY LIMIT

In Fig. 6, we illustrated the dependence of the discommensuration velocity v on the applied force $F_{\rm app}$, plotting the *normalized* velocity $\rho = va/D$ for convenience. For finite diffusivity D, the functions $v(F_{\rm app})$ and $\rho(F_{\rm app})$ are equivalent, but, as $D \to 0$, this is no longer the case. In this static-impurity limit, all finite velocities v correspond to $\rho = va/D = \infty$, while all finite values of ρ correspond to $v = D\rho/a = 0$. Since $F_{\rm drag}$ depends on v and D *only* through the combination $\rho = va/D$, then the entire contribution $F_{\rm drag}(\rho)$ is collapsed to the single point $v = 0$. Thus, in the static-impurity limit ($D \to 0$), the general force-velocity relationship consists of the following two branches:

$$\begin{aligned} &v = 0, \quad 0 \le F_{\rm app} \le F^* , \\ &v = v_0(F_{\rm app}), \quad 0 \le F_{\rm app} < \infty , \end{aligned} \tag{6.1}$$

where F^* is the maximum of the function $F_{\rm drag}(\rho)$ [i.e., $F^* = F_{\rm drag}(\rho^*)$], and $v_0(F)$ is the impurity-free force-velocity relationship discussed in the first paragraph of Sec. V.

Physically, Eqs. (6.1) mean that, as the applied force is increased from $F_{\rm app} = 0$, the discommensurations remained pinned ($v = 0$) to the static impurities. However, when the applied force finally reaches the threshold value F^*, the discommensurations suddenly break free and, after a transient acceleration, move with the velocity

$$\tilde{v} = v_0(F^*) . \tag{6.2}$$

Furthermore, after the discommensurations break free, they are governed by the impurity-free force-velocity relationship $v_0(F)$. Finally, we mention that this static impurity limit ($D \to 0$) is valid whenever D/a is small compared to all physically observable velocities v.

An analytic expression for F^* [which is the maximum value of Eq. (4.3)] cannot be found in general. However, such expressions can be found in the weak- and strong-interaction limits. As mentioned in Sec. IV, we have

$$\rho^* = \begin{cases} 1, & |\sigma| \ll 1 \\ 1/\ln|\sigma| , & |\sigma| \gg 1 , \end{cases} \tag{6.3}$$

which yields [from Eqs. (4.8) and (4.9)]

$$\begin{aligned} F^* &= F_{\rm drag}(\rho^*) \\ &= \begin{cases} C_0\sigma^2 kT/4, & |\sigma| \ll 1 \\ 2C_0 kTe^{|\sigma|}/(e|\sigma|\ln|\sigma|), & |\sigma| \gg 1 . \end{cases} \end{aligned} \tag{6.4}$$

The above results (6.1)–(6.4) are valid in general. More specifically, for the sine-Gordon force-velocity relationship (5.1), Eqs. (6.1) and (6.2) become

$$\begin{aligned} &v = 0, \quad 0 \le F_{\rm app} \le F^* , \\ &v = v_\infty [1 + (F_0/F_{\rm app})^2]^{-1/2}, \quad 0 \le F_{\rm app} < \infty , \end{aligned} \tag{6.5}$$

$$\tilde{v} = v_\infty [1 + (F_0/F^*)^2]^{-1/2} , \tag{6.6}$$

with F^* still given by Eq. (6.4). To connect these results with those of Sec. V, note that

$$F^* = \lim_{D \to 0} F_+ , \tag{6.7}$$

$$\tilde{v} = \lim_{D \to 0} D\tilde{\rho}_+ / a . \tag{6.8}$$

VII. APPLICATIONS

As our first example, we consider a charge-density-wave material at room temperature. For a material such as TaS_3 doped with Nb, the relevant physical parameters have the approximate values: $T = 300$ K, $v_\infty = 6 \times 10^5$ cm/sec, $a = 0.5$ nm, $E_0 = -3$ meV, $C_0 a = 10^{-3}$, $F_0 = 10^2$ eV/cm, $D_0 = 10^6$ cm^2/sec, and $Q_D = 2.5$ eV. In addition, these values yield: $C_0 = 2 \times 10^4$ cm^{-1}, $D = 10^{-36}$ cm^2/sec, $\rho_\infty = 3 \times 10^{34}$, and $\sigma = -0.1$. In particular, note that $\rho_\infty \gg 1$, as assumed in Secs. V and VI. Since $|\sigma| \ll 1$, then the relevant parameter for hysteresis is $\lambda = 2 \times 10^{32}$, and, since $\lambda \gg \lambda_c = 27$, this system exhibits pronounced hysteresis. Furthermore, since $D/a = 2 \times 10^{-29}$ cm/sec is extremely small compared to all physically observable velocities, we are clearly in the static-impurity limit. From Eqs. (6.4) and (6.6), we have

$$F^* = 1 \text{ eV/cm} , \tag{7.1}$$

$$\tilde{v}/v_\infty = 10^{-2} . \tag{7.2}$$

Thus, we see that the charge-density wave depins at a threshold electric field on the order of $E^* = 1$ V/cm, and, after a transient acceleration, the unpinned charge-density wave is moving at about 1% of the sound velocity. This charge-density wave is still in the linear regime of Eq. (6.5), the force-velocity relationship being $v = MF_{\rm app}$ with the mobility $M = 6 \times 10^3$ cm^2/eV sec.

Next, we consider ferroelectric domain walls near room temperature. For an ionic conductor such as $Ba_2NaNb_5O_{15}$, the relevant physical parameters have the approximate values (note the rather large diffusivity): $T = 300$ K, $v_\infty = 10^5$ cm/sec, $a = 0.5$ nm, $E_0 = -0.5$ eV, $C_0 a = 10^{-3}$, $D = 3 \times 10^{-4}$ cm^2/sec, and $M = 1$ cm^2/eV sec. In turn, these values yield: $C_0 = 2 \times 10^4$ cm^{-1}, $F_0 = 10^5$ eV/cm, $\rho_\infty = 20$, and $\sigma = -20$. Again, note that $\rho_\infty \gg 1$ (as required). Since $|\sigma| \gg 1$, then the relevant parameter for hysteresis is now $\Lambda = 2 \times 10^6$, and, since $\Lambda \gg \Lambda_c = e^2/2$, we again have pronounced hysteresis. However, since $D/a = 6 \times 10^3$ cm/sec, we are definitely *not* in the static-impurity limit.

From Eqs. (5.22)–(5.27), we have (using the results for case I):

$$F_+ = 2 \times 10^9 \text{ eV/cm} , \tag{7.3}$$

$$F_- = 2 \times 10^4 \text{ eV/cm} , \tag{7.4}$$

$$\rho_+ = 0.3 , \tag{7.5}$$

$$\rho_- = 5 , \tag{7.6}$$

$$\tilde{\rho}_+ = 20 , \tag{7.7}$$

$$\tilde{\rho}_- = 10^{-6} , \tag{7.8}$$

where the forces are per *atom* of the domain wall. These values correspond to the following electric fields and velocities: $E_+ = 2 \times 10^9$ V/cm, $E_- = 2 \times 10^4$ V/cm,

$v_+/v_\infty = 2\times10^{-2}$, $v_-/v_\infty = 0.2$, $\tilde{v}_+/v_\infty = 1$, and $\tilde{v}_-/v_\infty = 6\times10^{-8}$. Thus, we see that, for all physically observable domain-wall velocities, there are two coexisting force-velocity relationships. Furthermore, these two branches are separated by an unobtainable threshold field E_+. However, this does not mean that the upper (higher-velocity) branch cannot be reached. The results presented here are steady-state results. If the applied field is increased *slowly*, then the system will remain in steady-state on the lower branch of the force-velocity relationship. On the other hand, if the field is applied suddenly (or if an unequilibrated domain wall is injected into the system), then the system will not immediately be in steady state. In this case, the system will approach steady state, but the final state may lie on any available branch of the force-velocity relationship, depending on the *transient* behavior of the system. For fields between E_- and E_+, both branches may be populated by domain walls, with the fraction in the upper branch increasing from 0 to 1 as the applied field is increased from E_- to E_+.[21] In this situation, the *average* domain-wall velocity will increase faster than linearly with the applied field between E_- and E_+.

Finally, we consider grain boundaries at various temperatures. For a material such as Al doped with Fe, the relevant physical parameters have the approximate values: $v_\infty = 6\times10^5$ cm/sec, $a = 0.5$ nm, $E_0 = -0.2$ eV, $C_0 a = 10^{-3}$, $D_0 = 10^6$ cm^2/sec, $Q_D = 2.5$ eV, $M_0 = 10^2$ cm^2/eV sec, and $Q_M = 0.5$ eV. At room temperature, $T = 300$ K, these values yield: $C_0 = 2\times10^4$ cm^{-1}, $D = 10^{-36}$ cm^2/sec, $M = 4\times10^{-7}$ cm^2/eV sec, $F_0 = 2\times10^{12}$ eV/cm, $\rho_\infty = 3\times10^{34}$, and $\sigma = -8$ (again, $\rho_\infty \gg 1$, as required). Since $|\sigma| \gg 1$, then the relevant parameter for hysteresis is $\Lambda = 4\times10^{27}$, and, since $\Lambda \gg \Lambda_c = e^2/2$, we again have pronounced hysteresis. Furthermore, since $D/a = 2\times10^{-29}$ cm/sec is extremely small compared to all physically observable velocities, we are clearly in the static-impurity limit, and, from Eqs. (6.4) and (6.6), we have

$$F^* = 7\times10^4 \text{ eV/cm} , \tag{7.9}$$

$$\tilde{v} = 2\times10^{-2} \text{ cm/sec} , \tag{7.10}$$

where F^* is again the force per *atom* of the grain boundary. Thus, we see that, at room temperature, the grain boundaries depin at an applied force[22] of $F^* = 7\times10^4$ eV/cm, after which they are still in the linear force-velocity regime with the mobility $M = 4\times10^{-7}$ cm^2/eV sec.

As the temperature is increased, these results change substantially. At $T = 700$ K, for example, we have: $C_0 = 2\times10^4$ cm^{-1}, $D = 10^{-12}$ cm^2/sec, $M = 3\times10^{-2}$ cm^2/eV sec, $F_0 = 2\times10^7$ eV/cm, $\rho_\infty = 3\times10^{10} \gg 1$, and $\sigma = 3$. This yields $\Lambda = 10^7 \gg \Lambda_c = e^2/2$, so that we still have pronounced hysteresis. However, since we now have $D/a = 2\times10^{-5}$ cm/sec, we are no longer in the static-impurity limit. From Eqs. (5.22)–(5.27), we have (using the results for case III):

$$F_+ = 4\times10^3 \text{ eV/cm} , \tag{7.11}$$

$$F_- = 5 \text{ eV/cm} , \tag{7.12}$$

$$\rho_+ = 0.9 , \tag{7.13}$$

$$\rho_- = 4\times10^3 , \tag{7.14}$$

$$\tilde{\rho}_+ = 7\times10^6 , \tag{7.15}$$

$$\tilde{\rho}_- = 4\times10^{-4} , \tag{7.16}$$

with the latter four values corresponding to the following velocities: $v_+ = 2\times10^{-5}$ cm/sec, $v_- = 8\times10^{-2}$ cm/sec, $\tilde{v}_+ = 10^2$ cm/sec, and $\tilde{v}_- = 8\times10^{-9}$ cm/sec.

From these results, we see that, as the temperature is increased, allowing the impurities to diffuse, the hysteresis becomes much more evident (as opposed to the simple on/off switch at room temperature). At $T = 700$ K, there are two coexisting branches over much of the experimentally accessible range, and, above the threshold force $F_+ = 4\times10^3$ eV/cm, the grain boundaries depin from the impurities and move with the impurity-free mobility $M = 3\times10^{-2}$ cm^2/eV sec. Thus, of the examples considered here, grain boundaries at high temperatures appear to be the most promising system in which to observe all of the aspects of hysteresis.

VIII. CONCLUSIONS

In this paper, we have provided an analytical description of the interaction of moving discommensurations and diffusing impurities. For both misfit and elastic-modulus impurities, we have shown that the impurity-discommensuration interaction potential has the form given in Eq. (3.6). Then, for this typical interaction potential, we have evaluated the steady-state impurity concentration about a moving discommensuration. For an attractive interaction, this concentration is peaked at the discommensuration, with a small deficit leading it. For a repulsive interaction, there is a dip at the discommensuration, with a large excess piled up in front of it. In either case, the net excess concentration is positive for a moving discommensuration.

Next, we have found the drag force exerted by these impurities on the moving discommensuration. As the discommensuration velocity increases, this drag force increases linearly in the velocity, reaches a peak, and then falls off inversely with the velocity. For a weak impurity-discommensuration interaction, the drag force is a fairly simple function of velocity. However, for a strong interaction, the dependence on velocity becomes quite complex, with a large, sharp peak and a long tail.

Taking into account this drag force, we have then found the dependence of the discommensuration velocity on the applied force. For certain ranges of parameters, this force-velocity relationship exhibits hysteresis, which results from the pinning and depinning of the discommensurations to the impurities. At low fields, the discommensurations are pinned and move with a low mobility, but, at high fields, they are depinned and move with the much higher mobility of an impurity-free material. At intermediate fields, both of these behaviors coexist. Furthermore, the fields bounding this region of hysteresis depend very sensitively on the temperature, as well as the impurity-discommensuration interaction strength (when it exceeds the temperature). Also, when the impurity dif-

fusivity is very low, so that the impurities are static and cannot keep up with the moving discommensurations, this hysteresis represents a switch (at a single threshold field) between stationary, pinned discommensurations and unpinned discommensurations moving with the impurity-free mobility.

Finally, we have applied these results to three physical systems with very different behaviors. Charge-density waves with static impurities are easily depinned at room temperature, having a threshold field of only about 1 V/cm. On the other hand, ferroelectric domain walls with very mobile impurities have a fairly wide range of hysteresis, which encompasses most of the fields of experimental interest. As a result, these domain walls may populate both branches of the force-velocity relationship, allowing the average discommensuration velocity to increase faster than linearly with the applied field. Finally, grain boundaries show both of these behaviors. At room temperature, the impurities are static, and the grain boundaries act much like charge-density waves (but with a much larger threshold force for depinning). However, at higher temperatures, the impurities become mobile, leading to a fairly wide range of hysteresis, as for ferroelectric domain walls.

ACKNOWLEDGMENT

We gratefully acknowledge useful discussions with J. F. Scott and extend our appreciation for his careful reading of this manuscript.

APPENDIX

In deriving many of the results in the main body of this paper, we have made extensive use of the modified, incomplete γ function $\gamma^*(a,x)$.[16] Unfortunately, very few properties of this function can be found in standard mathematical handbooks.[23] Consequently, we summarize here the pertinent properties of this function. We begin by describing the function $\gamma^*(a,x)$ and indicating why it is preferable to the more common incomplete γ function $\gamma(a,x)$, whose properties are much more frequently tabulated.

For $a>0$, the standard (complete) γ function is defined by

$$\Gamma(a)=\int_0^\infty z^{a-1}e^{-z}dz \ . \tag{A1}$$

Furthermore, integrating by parts yields

$$\Gamma(a)=\frac{1}{a}\int_0^\infty z^a e^{-z}dz=\frac{1}{a}\Gamma(a+1) \ , \tag{A2}$$

and this recursion relation can be used to define $\Gamma(a)$ for $a<0$ (but not for nonpositive integers).

Similarly, for $a>0$ and $x\geq 0$, the incomplete γ function is defined by[16]

$$\gamma(a,x)=\int_0^x z^{a-1}e^{-z}dz \ , \tag{A3}$$

and it too can be extended to $a<0$ by integrating by parts (but, again, not to nonpositive integers). However, for $x<0$, Eq. (A3) is not well defined, because of the factor z^{a-1} with $z<0$ (unless a is a positive integer). Consequently, one defines the modified, incomplete γ function (for $a>0$ and $x\geq 0$):[16]

$$\gamma^*(a,x)=\gamma(a,x)/x^a\Gamma(a) \ . \tag{A4}$$

The factor x^a allows (A3) to be extended to $x<0$, since z^{a-1} becomes $(z/x)^{a-1}$, and z/x is always positive. Furthermore, the factor $\Gamma(a)$ cancels the divergence in $\gamma(a,x)$ for nonpositive integers a, so that $\gamma^*(a,x)$ is well defined there. Thus, $\gamma^*(a,x)$ can be defined for all real a and x (actually, for all complex a and x as well).

We must now find expressions for $\gamma^*(a,x)$ which are valid for all a and x. Inserting Eq. (A3) into Eq. (A4) and changing variables leads to

$$\gamma^*(a,x)=\frac{1}{\Gamma(a)}\int_0^1 z^{a-1}e^{-xz}dz \ . \tag{A5}$$

This expression is valid for all x, but only for $a>0$. To extend Eq. (A5) to $a\leq 0$, we again integrate by parts, yielding

$$\gamma^*(a,x)=e^{-x}/\Gamma(a+1)+x\gamma^*(a+1,x) \ . \tag{A6}$$

This recursion relation can be used to find $\gamma^*(a,x)$ for all $a\leq 0$.

Having defined $\gamma^*(a,x)$ and motivated its use, we now catalog some of its useful properties. We begin with the series expansion

$$\gamma^*(a,x)=\sum_{n=0}^{\infty}\frac{(-x)^n}{n!(a+n)\Gamma(a)} \tag{A7}$$

(which is valid for all complex a and x). Note that, if a is a nonpositive integer, $\Gamma(a)$ is infinite, but $(a+n)\Gamma(a)$ is finite for the term $n=-a$. Thus, in this case, only a single term in the above sum is nonzero, and we have

$$\gamma^*(-N,x)=x^N \quad (N=0,1,2,\ldots) \ . \tag{A8}$$

Next, we give two useful recursion relations (for N a positive integer):

$$\gamma^*(a,x)=e^{-x}\sum_{n=0}^{N-1}\frac{x^n}{\Gamma(a+n+1)}+x^N\gamma^*(a+N,x) \ , \tag{A9}$$

$$\gamma^*(a,x)=-e^{-x}\sum_{n=1}^{N}\frac{x^{-n}}{\Gamma(a-n+1)}+x^{-N}\gamma^*(a-N,x) \ . \tag{A10}$$

Finally, we state the useful result

$$\frac{\partial^n\gamma^*(a,x)}{\partial x^n}=(-1)^n\frac{\Gamma(a+n)}{\Gamma(a)}\gamma^*(a+n,x) \ . \tag{A11}$$

Our main use of $\gamma^*(a,x)$ is in the evaluation of the integrals encountered in the main body of this paper. Through changes of variables, these integrals can be written in terms of the following four results:

$$\int_\mu^\nu z^{a-1}e^{-xz}dz=\Gamma(a)[\nu^a\gamma^*(a,\nu x)-\mu^a\gamma^*(a,\mu x)] \quad (\nu>\mu>0) \ , \tag{A12}$$

$$\int_0^\nu z^{a-1}e^{-xz}dz=\nu^a\Gamma(a)\gamma^*(a,\nu x) \quad (\nu,a>0) \ , \tag{A13}$$

$$\int_{\mu}^{\infty} z^{a-1}e^{-xz}dz=\Gamma(a)[x^{-a}-\mu^{a}\gamma^{*}(a,\mu x)] \quad (\mu,x>0)\ , \tag{A14}$$

$$\int_{0}^{\infty} z^{a-1}e^{-xz}dz=x^{-a}\Gamma(a) \quad (a,x>0)\ . \tag{A15}$$

The expressions involving these modified, incomplete γ functions become more transparent in various limiting cases. In examining these limits, we make use of several asymptotic forms of $\gamma^{*}(a,x)$, which we now discuss. A series representation of $\gamma^{*}(a,x)$ which is useful for $|a|\gg 1$ is

$$\gamma^{*}(a,x)=e^{-x}\sum_{n=0}^{\infty}\frac{x^{n}}{\Gamma(a+n+1)}\ . \tag{A16}$$

On the other hand, for $|a|\ll 1$, it is convenient to use the series

$$\gamma^{*}(a,x)=\frac{1}{\Gamma(1+a)}\left[1+x\sum_{n=1}^{\infty}a^{n}G_{n}(x)\right]\ , \tag{A17}$$

$$G_{n}(x)=\frac{1}{n!}\int_{0}^{1}e^{-xz}(\ln z)^{n}dz\ . \tag{A18}$$

For the asymptotic result, it is sufficient to stop at the term

$$G_{1}(x)=\frac{1}{x}[\mathrm{Ei}(-x)-\ln|x|-\gamma]\ . \tag{A19}$$

Here, $\mathrm{Ei}(z)$ is the exponential-integral function,[16] and γ is Euler's constant.

A series representation useful for $|x|\ll 1$ is given by Eq. (A7). On the other hand, for $|x|\gg 1$, there is no useful series representation. However, we can use the *asymptotic* series[24]

$$\gamma^{*}(a,x)=\begin{cases} x^{-a}-e^{-x}\displaystyle\sum_{n=1}^{M}\frac{1}{x^{n}\Gamma(a-n+1)}, & x>0 \text{ or } x<0 \text{ and } a \text{ an integer} \\ -e^{-x}\displaystyle\sum_{n=1}^{M}\frac{1}{x^{n}\Gamma(a-n+1)}, & x<0 \text{ and } a \text{ not an integer} \end{cases} \tag{A20}$$

(where the upper limit M is simply a reminder that the series is only asymptotic). Note that, for a an integer, the above series terminates, and, thus, it is not just an asymptotic series. Furthermore, if $x>0$ ($x<0$), then x^{-a} is the largest (smallest) term as $|x|\to\infty$. The expressions (A20) lead to the asymptotic forms (for $|x|\gg 1$)

$$\gamma^{*}(a,x)=\begin{cases} x^{-a}-\dfrac{1}{x\Gamma(a)}e^{-x}\left[1+\dfrac{a-1}{x}+\cdots\right], & x>0 \\ \dfrac{1}{|x|\Gamma(a)}e^{|x|}\left[1-\dfrac{a-1}{|x|}+\cdots\right], & x<0 \text{ and } a\neq 1,\ 0,\ -1,\ \ldots \\ \dfrac{1}{|x|}e^{|x|}-\dfrac{1}{|x|}, & x<0 \text{ and } a=1 \\ x^{-a}, & x<0 \text{ and } a=0,-1,-2,\ \ldots\ . \end{cases} \tag{A21}$$

Equation (A11) shows that $\partial\gamma^{*}(a,x)/\partial x$ is simply related to $\gamma^{*}(a,x)$ itself. However, this is not the case for $\partial\gamma^{*}(a,x)/\partial a$, which we will denote by $\gamma_{1}^{*}(a,x)$. In this paper, $\gamma_{1}^{*}(a,x)$ is encountered only for integer values of a, in which case, we have

$$\gamma_{1}^{*}(N,x)=\begin{cases} x^{-N}\left[\mathrm{Ei}(-x)-\ln|x|+e^{-x}\displaystyle\sum_{n=0}^{N-1}\frac{\psi(n+1)}{n!}x^{n}\right], & N=1,2,\ldots \\ x^{|N|}\left[\mathrm{Ei}(-x)-\ln|x|+\dfrac{1}{x}e^{-x}\displaystyle\sum_{n=0}^{|N|-1}\frac{n!}{(-x)^{n}}\right], & N=0,-1,\ldots\ , \end{cases} \tag{A22}$$

where $\psi(z)$ is the digamma function.[16] For nonnegative integers n, we have

$$\psi(n+1)=\sum_{m=1}^{n}\frac{1}{m}-\gamma\ . \tag{A23}$$

Finally, we give the asymptotic forms for $\gamma_{1}^{*}(-N,x)$ where $N=1,2,\ldots$. A series representation useful for $|x|\ll 1$ is

$$\gamma_1^*(-N,x)=(-1)^N N!\left[-\frac{1}{N}+\sum_{\substack{n=1\\n\neq N}}^{\infty}\frac{(-x)^n}{n!(n-N)}\right]-x^N\psi(N+1)\ . \tag{A24}$$

For $|x|\gg 1$, we must again settle for an asymptotic series, and we find

$$\gamma_1^*(-N,x)=\begin{cases}-x^N\ln x-\dfrac{(-1)^N}{x}e^{-x}\displaystyle\sum_{n=0}^{M}\frac{(N+n)!}{(-x)^n}, & x>0\\[2ex] \dfrac{(-1)^N}{|x|}e^{|x|}\displaystyle\sum_{n=0}^{M}\frac{(N+n)!}{|x|^n}, & x<0\ .\end{cases} \tag{A25}$$

[1]L. J. Sham and B. R. Patton, Phys. Rev. B **13**, 3151 (1976).

[2]Y. Imry and S.-K. Ma, Phys. Rev. Lett. **35**, 1399 (1975).

[3]P. W. Young and J. F. Scott, Phase Transitions **6**, 175 (1986).

[4]K. T. Aust and J. W. Rutter, Trans. Am. Inst. Min. Metall. Pet. Eng. **215**, 119 (1959).

[5]M. B. Fogel, S. E. Trullinger, A. R. Bishop, and J. A. Krumhansl, Phys. Rev. B **15**, 1578 (1977).

[6]H. Fukuyama and P. A. Lee, Phys. Rev. B **17**, 535 (1978).

[7]H. Fukuyama, J. Phys. Soc. Jpn. **45**, 1474 (1978).

[8]K. Nakanishi, J. Phys. Soc. Jpn. **46**, 1434 (1979).

[9]J. W. Cahn, Acta. Metall. **10**, 789 (1962).

[10]J. Frenkel and T. Kontorova, Phys. Z. Sowjetunion **13**, 1 (1938) [J. Phys. (Moscow) **1**, 137 (1939)].

[11]J. H. Wiener, Phys. Rev. **136**, 863 (1964).

[12]Actually, in the absence of impurities, we must have $\Delta(u)\equiv 0$ and $\beta(u)\equiv\beta$. We then rescale to make $\beta=1$ for convenience.

[13]This is the minimum-energy solution of the Ginzburg-Landau Hamiltonian $H=\int_{-\infty}^{\infty}(\phi_u^2/2-\phi^2/2+\phi^4/4)du$ with the antisymmetric boundary conditions $\phi(-\infty)=-\phi(\infty)=1$, after the appropriate shifting and rescaling.

[14]C. H. P. Lupis, *Chemical Thermodynamics of Materials* (North-Holland, New York, 1983), p. 160.

[15]For simpler potentials, similar results have been obtained by R. Fuentes-Samaniego and J. P. Hirth, Phys. Status Solidi B **125**, 147 (1984).

[16]*Handbook of Mathematical Functions,* edited by M. Abramowitz and I. A. Stegun (Dover, New York, 1972), Chaps. 5 and 6.

[17]J. P. Hirth and J. Loethe, *Theory of Dislocations* (Wiley, New York, 1982), Chap. 18.

[18]N. F. Mott, Proc. Phys. Soc. London **60**, 391 (1948).

[19]It is, of course, only the steady-state value that is discontinuous. The system "jumps" between the two values through a continuous, transient behavior.

[20]N. F. Pedersen and D. Welner, Phys. Rev. B **29**, 2551 (1984).

[21]Of course, this fraction may depend on more than just the value of the electric field E.

[22]For grain boundaries, this force is typically associated with a release of strain energy as a boundary moves. As a result, its relation to an applied field is not straightforward. Thus, for grain boundaries, we give our results only in terms of applied forces.

[23]Such handbooks generally discuss the standard, incomplete γ function $\gamma(a,x)$ instead.

[24]When a function $F(x)$ is approximated by a finite series $F_n(x)=\sum_{m=1}^{n}f_n(x)$, one generally means that $\lim_{n\to\infty}F_n(x)=F(x)$. However for an asymptotic series, $\lim_{n\to\infty}F_n(x)$ is divergent, and one means that $\lim_{x\to\infty}F_n(x)/F(x)=1$. In this paper, asymptotic series will have an (arbitrary) upper limit M to distinguish them from standard infinite series (which have the upper limit ∞).